

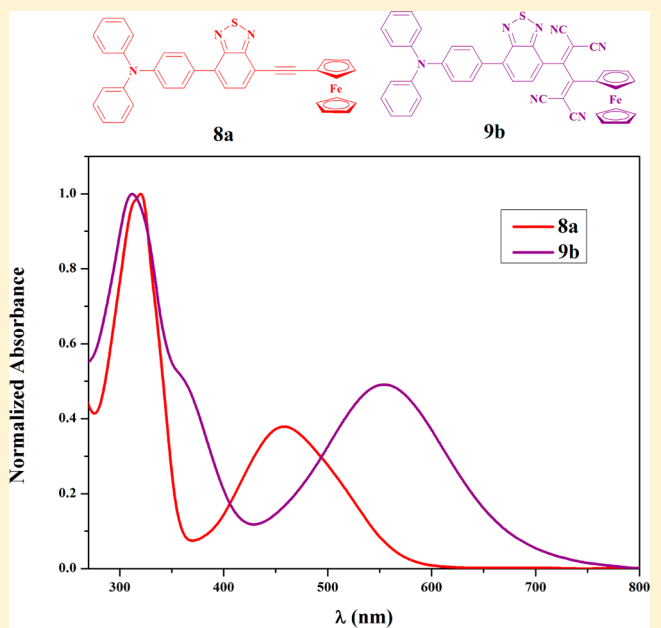
Aryl-Substituted Unsymmetrical Benzothiadiazoles: Synthesis, Structure, and Properties

Rajneesh Misra,* Prabhat Gautam, and Shaikh M. Mobin

Department of Chemistry, Indian Institute of Technology Indore, Indore 452 017, India

S Supporting Information

ABSTRACT: A family of unsymmetrical donor–acceptor, ferrocenyl-substituted benzothiadiazoles of types $D_1-\pi-A-\pi-D_2$, $D_1-\pi-A_1-\pi-A_2$, $D_1-A-\pi-D_2$, and $D_1-A_1-A_2-D_2$, bearing a variety of electron-donating and electron-withdrawing groups, were designed and synthesized. Their photophysical, electrochemical, and computational properties were explored, which show strong donor–acceptor interaction. The presence of electron-rich units anthracene (**6f**) and triphenylamine (**6h**), and an electron-deficient unit 1,1,4,4-tetracyanobuta-1,3-diene (TCBD) (**9b**) results in lowering of the band gap, which leads to a red shift of the absorption spectrum in these benzothiadiazole systems. The single crystal structures of **6c**, **6g**, **7a**, and **7b** are reported, which show marvelous supramolecular interactions.



INTRODUCTION

The design and synthesis of organic π -conjugated donor–acceptor systems continues to create a great amount of interest because of their application in organic photovoltaics (OPV) and nonlinear optics (NLO).¹ The properties of the donor–acceptor system can be modulated either by increasing the donor and acceptor strength or by varying the π -linker between the donor and the acceptor.² A wide variety of donors and acceptors have been used for the synthesis of $D-\pi-A$ type of systems.³ 2,1,3-Benzothiadiazole (BTD) is a strong acceptor due to its high electron affinity.⁴ Ferrocene is a strong electron donor and highly stable. Our group is interested in the design and synthesis of ferrocene-based donor–acceptor molecular systems for a variety of photonic applications.^{5,6} Recently we have reported the synthesis of ferrocene-substituted symmetrical and unsymmetrical BTD systems of types $D-\pi-A-\pi-D$, $D-\pi_1-A-\pi_2-D$, and $D-\pi_1-A-\pi_2-A-\pi_1-D$.^{7,8} In continuation of this work, we were further interested in the design and synthesis of unsymmetrical BTDs having different donors/acceptors of varying strengths and to see their effect on the donor–acceptor interaction. In this contribution, we wish to report unsymmetrical donor–acceptor systems of the types $D_1-\pi-A-\pi-D_2$, $D_1-\pi-A_1-\pi-A_2$, $D_1-A-\pi-D_2$, and $D_1-A_1-A_2-D_2$. Three sets of mono-bromobenzothiadiazoles **3a**, **4a**, and **5a** were

designed and synthesized by the Sonogashira, Suzuki, and Ullmann coupling reactions, respectively. These mono-bromobenzothiadiazoles (**3a**, **4a**, and **5a**) were further subjected to the Sonogashira cross-coupling reaction, which resulted in unsymmetrical BTDs. The unsymmetrical benzothiadiazoles **7a** and **8a** with a monoethyne spacer were subjected to [2 + 2] cycloaddition reaction with tetracyanoethene (TCNE), followed by ring-opening, which resulted in 1,1,4,4-tetracyanobuta-1,3-diene (TCBD) bridged unsymmetrical benzothiadiazoles **9a** and **9b**.

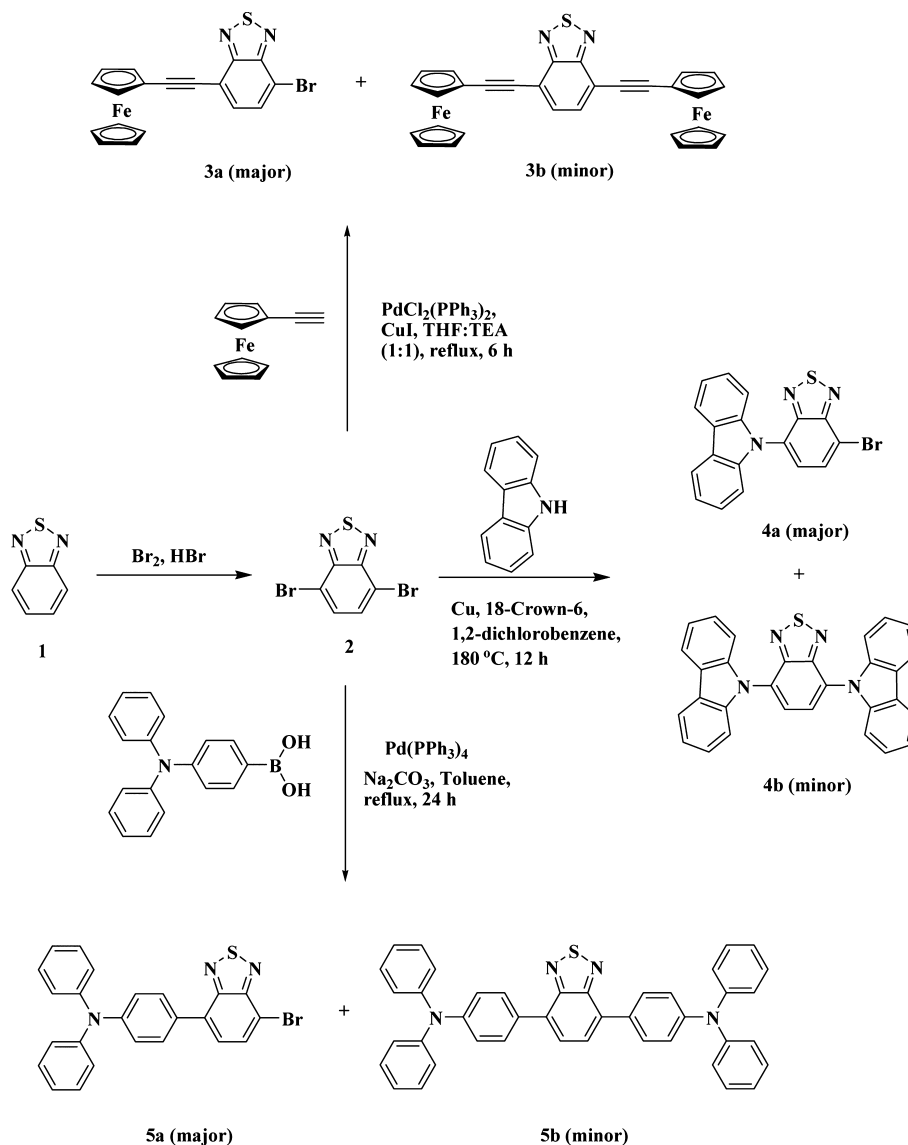
RESULT AND DISCUSSION

The synthesis of unsymmetrical benzothiadiazoles **6a–6h**, **7a–7c**, **8a–8c**, **9a**, and **9b** are outlined in Schemes 2–4. The dibromo-BTD **2** was synthesized by the bromination reaction of the BTD **1**.⁹ The Pd-catalyzed Sonogashira coupling reaction of ethynylferrocene and dibromo-BTD **2** resulted in 4-bromo-7-ferrocenylethynylbenzo[1,2,5]thiadiazole (**3a**) in 60% yield (Scheme 1).⁸ The Ullmann coupling reaction of carbazole and dibromo-BTD **2** resulted in 4-(9-carbazolyl)-7-bromo-2,1,3-benzothiadiazole (**4a**) in 40% yield (Scheme 1).¹⁰ The Pd-catalyzed Suzuki coupling reaction of the dibromo-BTD **2** and

Received: September 24, 2013

Published: November 26, 2013

Scheme 1. Synthetic Route for Mono-bromobenzo[1,2,5]thiadiazoles 3a, 4a, and 5a



4-(*N,N*-diphenylamino)-1-phenylboronic acid resulted in [4-(7-bromo-benzo[1,2,5]thiadiazol-4-yl)phenyl]diphenyl-amine (5a) in 50% yield (Scheme 1).¹¹

The precursors 3a, 4a, and 5a were further subjected to Sonogashira coupling reaction, which resulted in unsymmetrical BTDs. To study the effect of the aryl substituents with enhanced conjugation on the unsymmetrical ferrocenyl-BTD, a series of aromatic terminal alkynes were selected with one (10a–10c), two (10d and 10e), and three (10f–10h) aromatic rings. The Sonogashira cross-coupling reaction of the bromo-BTD 3a with the respective aryl-acetylenes (10a–10h) resulted in BTDs 6a–6h in 40–70% yield (Scheme 2).

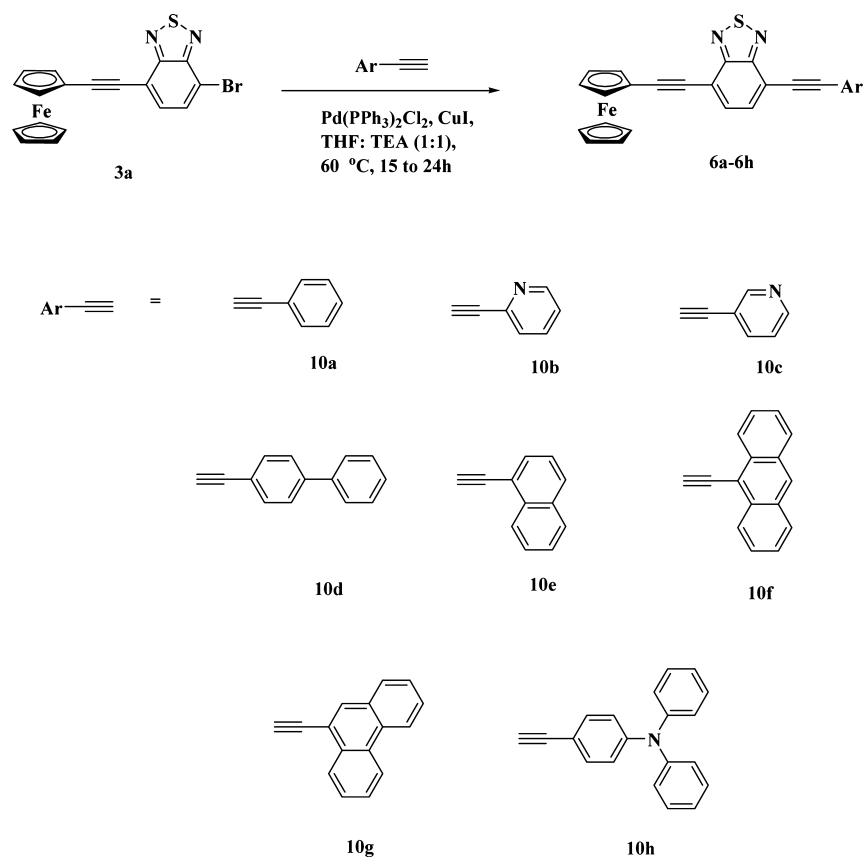
To explore the effect of variation of the π -bridge, a set of ethynyl-substituted ferrocenes, namely, ethynylferrocene (11a), 4-ferrocenylphenylacetylene (11b), and 4-ethynyl-phenylethynyl-ferrocene (11c), were synthesized and subjected to Sonogashira cross-coupling reaction with 4-(9-carbazolyl)-7-bromo-2,1,3-benzothiadiazole (4a), and [4-(7-bromo-benzo[1,2,5]thiadiazol-4-yl)phenyl]diphenyl-amine (5a). The Sonogashira coupling of the BTDs 4a and 5a with the respective ferrocenyl-acetylenes

resulted in compounds 7a–7c, and 8a–8c in 60–70% yield, respectively (Scheme 3).

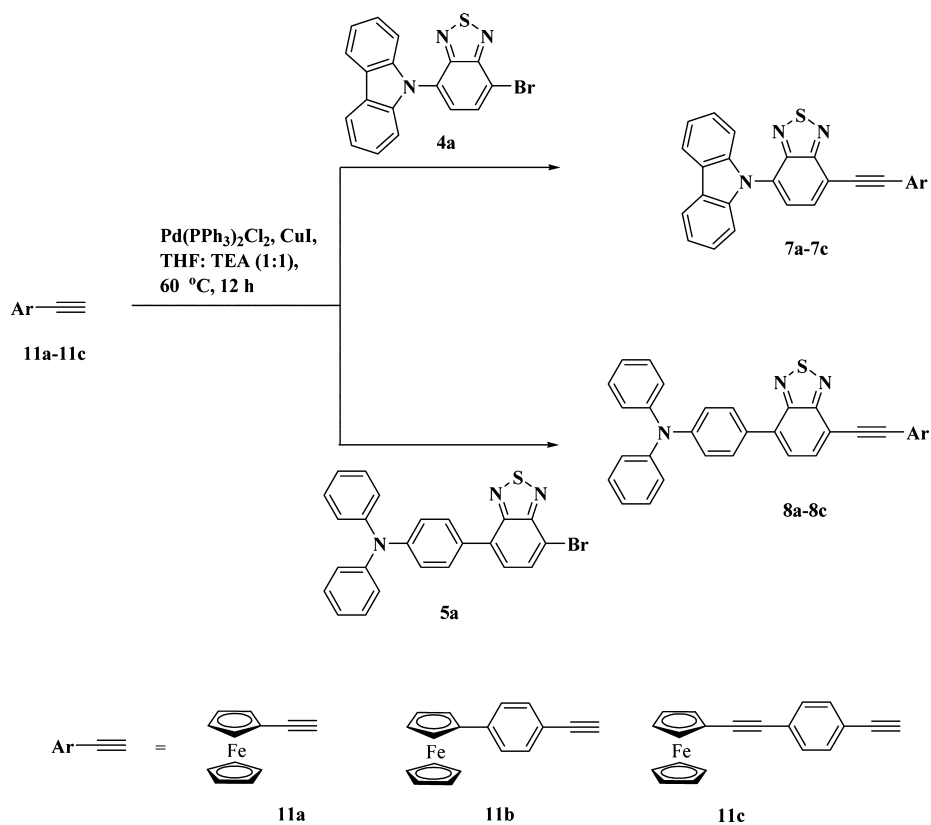
The 1,1,4,4-tetracyanobuta-1,3-diene (TCBD) bridged unsymmetrical BTDs 9a and 9b were synthesized via [2 + 2] cycloaddition reaction of the ferrocenyl-substituted BTDs 7a and 8a with tetracyanoethene (12) to form an intermediate cyclobutene that subsequently undergoes ring-opening (Scheme 4).¹² The purification of the unsymmetrical BTDs 6a–6h, 7a–7c, 8a–8c, 9a, and 9b was achieved by column chromatography. All the unsymmetrical BTDs were well-characterized by ¹H and ¹³C NMR and HRMS techniques. The BTDs 6c, 6g, 7a, and 7b were also characterized by single-crystal X-ray diffraction.

Thermogravimetric Analysis. The thermal properties of the unsymmetrical benzothiadiazoles 6a–6h, 7a–7c, 8a–8c, 9a, and 9b were investigated by the thermogravimetric analysis (TGA) at a heating rate of 10 °C min⁻¹, under a nitrogen atmosphere (Figure 1). The decomposition temperatures for 10% weight loss in the BTDs 6b–6h was above 450 °C, whereas the BTD 6a with the phenyl substituent shows the 10% weight loss at 249 °C. This reflects that the heteroaryl, biaryl, and the polycyclic aromatic substituted BTDs show higher thermal

Scheme 2. Synthesis of Unsymmetrical Benzothiadiazoles 6a–6h



Scheme 3. Synthesis of Benzothiadiazoles 7a–7c and 8a–8c



Scheme 4. Synthesis of Benzothiadiazoles 9a and 9b

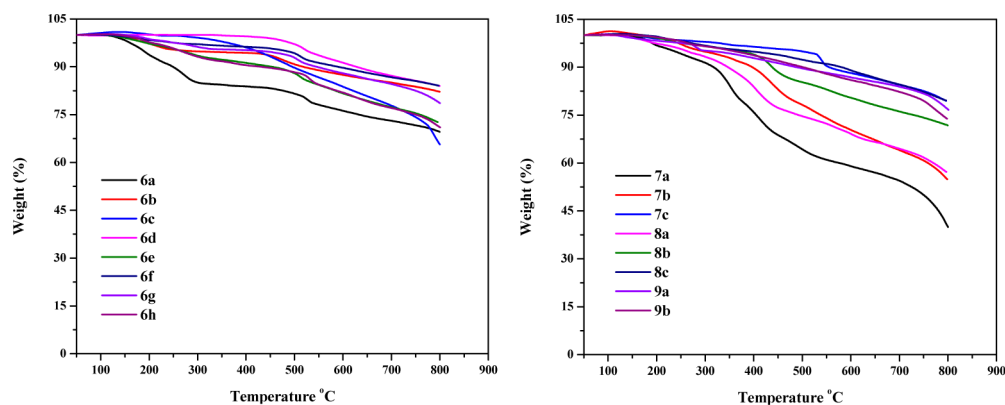
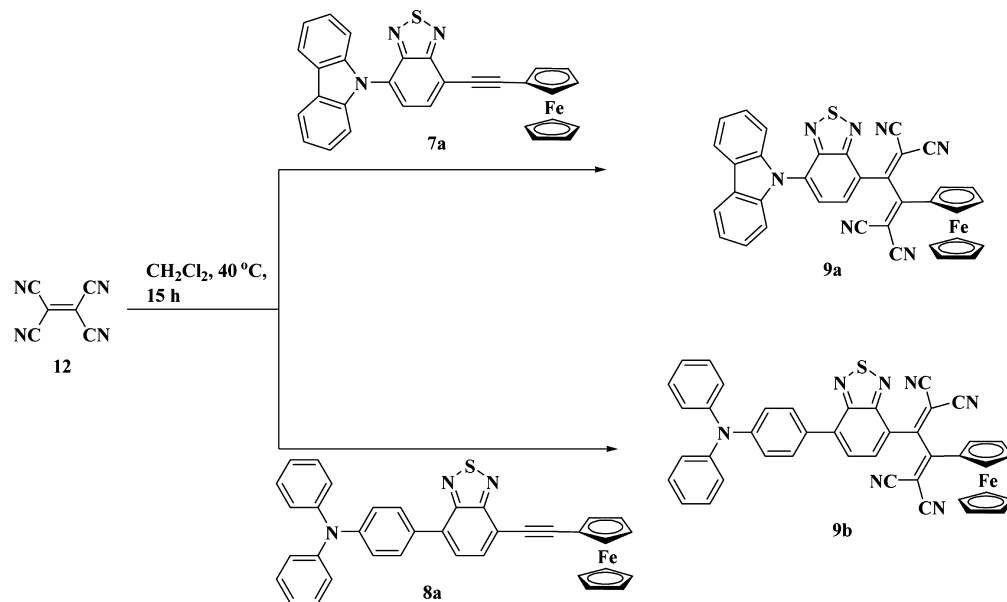


Figure 1. TGA plots of unsymmetrical BTDs 6a–6h, 7a–7c, 8a–8c, 9a, and 9b at a heating rate of $10\text{ }^\circ\text{C min}^{-1}$, under a nitrogen atmosphere.

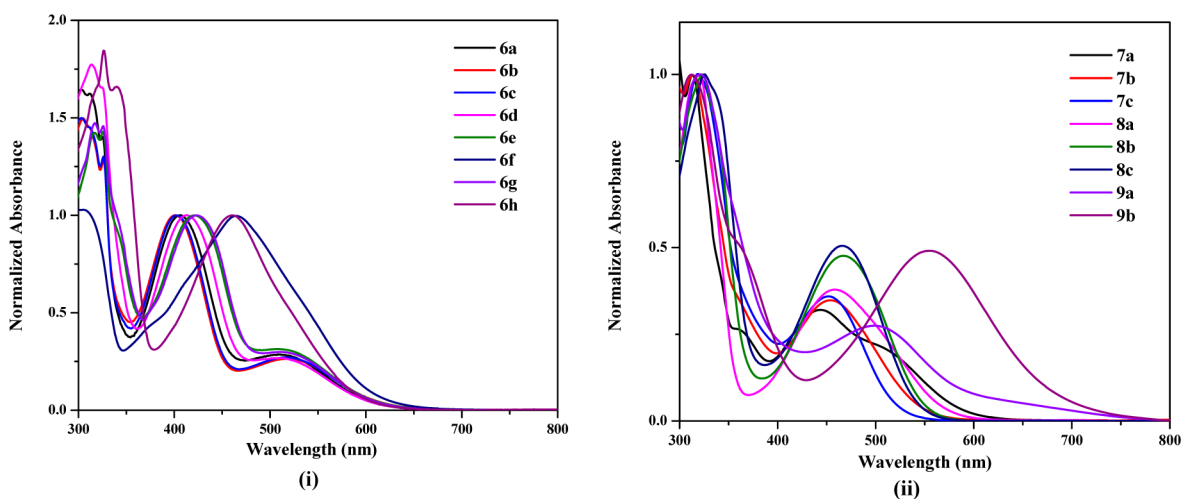


Figure 2. Normalized electronic absorption spectra of (i) benzothiadiazoles 6a–6h and (ii) benzothiadiazoles 7a–7c, 8a–8c, 9a, and 9b in dichloromethane at $1.0 \times 10^{-6}\text{ M}$ concentration.

stability. The BTDs 7a–7c and 8a–8c exhibit the 10% weight loss above $300\text{ }^\circ\text{C}$. The trend observed in the decomposition temperature follows the order $8\text{c} > 7\text{c} > 8\text{b} > 7\text{b} > 8\text{a} > 7\text{a}$. The

extension of the π -bridge between the ferrocene and the BTD unit results in increased thermal stability. The incorporation of a 1,1,4-tetracyanobuta-1,3-diene (TCBD) bridge results in

Table 1. Photophysical and Thermal Properties of the Benzothiadiazoles 6a–6h, 7a–7c, 8a–8c, 9a, and 9b

compound	photophysical data ^a		T_d (°C) ^b	compound	photophysical data ^a		T_d (°C) ^b
	λ_{abs} (nm)	ϵ (M ⁻¹ cm ⁻¹)			λ_{abs} (nm)	ϵ (M ⁻¹ cm ⁻¹)	
ferrocene	-	-					
6a	406	32 791	249	7a	443	35 138	328
	509	9324			520	sh	
6b	399	85 328	535	7b	453	47 855	411
	511	22 404					
6c	402	78 216	506	7c	454	62 777	604
	515	20 963					
6d	413	55 533	646	8a	458	37 842	359
	512	14 750					
6e	421	54 400	471	8b	466	51 474	449
	521	sh					
6f	465	67 550	611	8c	467	84 788	625
6g	423	58 074	563	9a	502	46 178	549
	514	sh					
6h	460	58 729	462	9b	554	61 482	543

^aAbsorbance measured in dichloromethane at 1×10^{-6} M concentration. sh: shoulder; λ_{abs} : absorption wavelength; ϵ : extinction coefficient.

^bDecomposition temperatures for 10% weight loss at a heating rate of $10 \text{ }^\circ\text{C min}^{-1}$, under a nitrogen atmosphere.

greater thermal stability in BTDs **9a** and **9b** compared to the ethyne bridged BTDs **7a** and **8a**. The decomposition temperatures for 10% weight loss is above $500 \text{ }^\circ\text{C}$ for TCBD-bridged BTDs **9a** and **9b**.

Photophysical Properties. The UV–vis absorption spectra of the unsymmetrical benzothiadiazoles were recorded in dichloromethane at room temperature (Figure 2), and the data are compiled in Table 1. The unsymmetrical BTDs show the characteristic absorption band between 300–340 nm due to the BTD unit.¹³

The BTDs **6a–6h** show the presence of a lower-energy absorption band between 399 and 465 nm, corresponding to the $\pi \rightarrow \pi^*$ transition, and between 509 and 521 nm attributed to the charge-transfer (CT) transitions.^{7,8,14} The red shift in the absorption maxima for the lower-energy $\pi \rightarrow \pi^*$ absorption band follows the order **6f** > **6h** > **6g** > **6e** > **6d** > **6a** > **6c** > **6b**. The magnitude in red shift observed for BTDs **6a–6h** is a function of the aryl substituent attached to the BTD core. A comparison of the absorption data reveals that the increase in the number of aromatic rings from one (**6a–6c**), two (**6d**, **6e**), and three (**6f–6h**) leads to a regular increase in the red shift of the absorption maxima due to enhancement of π -conjugation. The mode of conjugation in the aryl substituents also affects the absorption bands. The BTDs with naphthalene **6e** and anthracene **6f** substituents exhibit a red shift compared to the biphenyl **6d** and phenanthrene **6g** substituted BTDs, respectively. The BTDs **6a–6d** exhibit distinct a CT band between 509 and 515 nm, whereas **6e** and **6g** show in the form of a shoulder between 512 and 521 nm. The lower-energy electronic absorption maxima are broad in BTDs **6f** and **6h** due to the overlap with the charge-transfer absorption.^{8,15} The BTDs **7a–7c**, **8a–8c**, **9a**, and **9b** show the lower-energy absorption band between 443 and 554 nm. The BTD **7a** exhibits a CT band as a shoulder at 520 nm. The BTDs **7b**, **7c**, **8a–8c**, **9a**, and **9b** exhibit broadening of the lower-energy electronic absorption band, which can be attributed to the overlap of the lower-energy $\pi \rightarrow \pi^*$ transition with the CT band. The lower-energy electronic absorption band shows a bathochromic shift with the enhancement of conjugation length. The incorporation of a 1,1,4,4-tetracyanobuta-1,3-diene (TCBD) π -bridge in BTDs **9a** and **9b** results in substantial bathochromic shift of the lower-energy electronic absorption band compared to

BTDs **7a** and **8a**. The trend in the bathochromic shift follows the order **9b** > **9a** > **8a** > **7a**. This reveals strong donor–acceptor interaction in the TCBD π -bridge in BTDs **9a** and **9b**. The effect of systematic variation of π -conjugation through aryl substitution and the π -bridge is also reflected from the colored solution of these unsymmetrical BTDs **6a–6h**, **7a–7c**, **8a–8c**, **9a**, and **9b** (Figure 3).

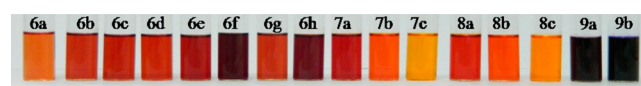


Figure 3. Unsymmetrical benzothiadiazoles **6a–6h**, **7a–7c**, **8a–8c**, **9a**, and **9b** at 1×10^{-4} M concentration in dichloromethane.

The emission studies of the unsymmetrical BTDs show complete quenching of the fluorescence.

Theoretical Calculations. DFT calculations were performed on the unsymmetrical benzothiadiazoles **6a–6h**, **7a–7c**, **8a–8c**, **9a**, and **9b** to explore the effect of the aryl substituents on the electronic structure of the unsymmetrical ferrocenyl-BTDs. The contours of the HOMO, and LUMO of BTDs **6a–6h**, **7a–7c**, **8a–8c**, **9a**, and **9b** are shown in Figures 4 and 5.

The HOMO orbitals are localized over the ferrocene, the aryl substituent, and the hydrocarbon portion of the BTD, whereas the LUMO orbitals are mainly concentrated on the BTD unit.^{8,16} The comparison of the HOMOs of BTDs **6d** and **6e** reveals greater delocalization of the HOMO orbital on the naphthalene unit compared to the biphenyl unit. Similarly, the anthracene unit in BTD **6f** shows better delocalization in the HOMO orbital, compared to the phenanthrene-substituted BTD **6g**. The presence of electron-rich substituents anthracene and triphenylamine on the BTDs **6f** and **6g** lowers the contribution of ferrocene in the HOMO. The band gap in BTDs **6a–6h** follows the order **6b** > **6c** \cong **6a** > **6d** > **6e** > **6g** > **6h** > **6f**, which is reflected in their electronic absorption. The band gaps in BTDs **7a–7c** and **8a–8c** were found to be inversely proportional to the conjugation length. In the HOMO of BTDs **8a–8c**, the contribution of the ferrocene unit is reduced with the extension of the π -bridge. The band gap in BTDs **7a–7c** and **8a–8c** follows the order **7a** > **7b** > **7c** and **8a** > **8b** > **8c**. The observed trend

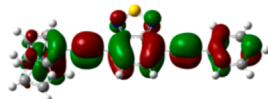
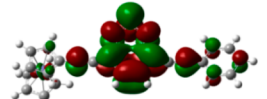
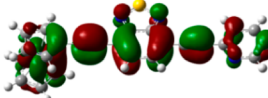
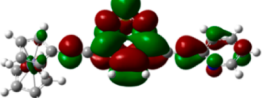
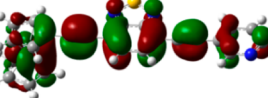
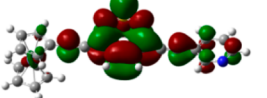
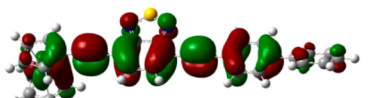
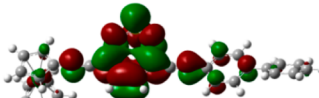
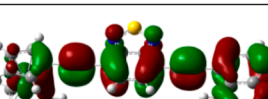
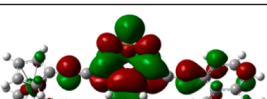
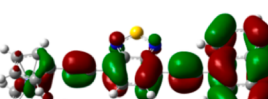
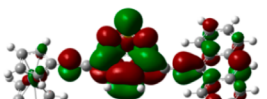
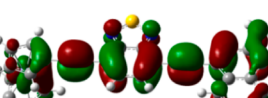
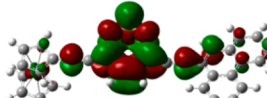
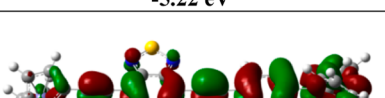
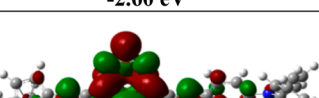
BTD	HOMO	LUMO	Calculated Band gap (eV)	Optical Band gap (eV) ^a
6a	 -5.29 eV	 -2.57 eV	2.72	2.16
6b	 -5.38 eV	 -2.65 eV	2.73	2.17
6c	 -5.41 eV	 -2.69 eV	2.72	2.15
6d	 -5.25 eV	 -2.58 eV	2.67	2.13
6e	 -5.23 eV	 -2.60 eV	2.63	2.11
6f	 -5.00 eV	 -2.66 eV	2.34	2.02
6g	 -5.22 eV	 -2.60 eV	2.62	2.09
6h	 -4.91 eV	 -2.48 eV	2.43	2.06

Figure 4. HOMO and LUMO frontier orbitals of unsymmetrical benzothiadiazoles **6a–6h** at the B3LYP/6-31G** level for C, N, S, and H, and the LanL2DZ level for Fe. (^a) Determined from the onset wavelength of the UV–vis absorption.

supports the electronic absorption behavior of BTDs **7a–7c** and BTDs **8a–8c**.

The 1,1,4,4-tetracyanobuta-1,3-diene (TCBD) π -bridge in **9a** and **9b** lowers the band gap, which results in a bathochromic shift of the electronic absorption spectra. The trend in the energy gap follows the order **7a** > **8a** > **9a** > **9b**.

Electrochemical Properties. The electrochemical behavior of the BTDs **6a–6h**, **7a–7c**, **8a–8c**, **9a**, and **9b** were explored by the cyclic voltammetric (CV) analysis in dry dichloromethane

(DCM) solution at room temperature using tetrabutylammoniumhexafluorophosphate (TBAPF₆) as a supporting electrolyte. The electrochemical data are listed in Table 2, and the representative cyclic voltammograms are shown in Figure 6, and Figure S2 (Supporting Information). In general, the unsymmetrical ferrocenyl-substituted BTDs show one reversible oxidation wave in the region of 0.04–0.42 V, corresponding to the oxidation of ferrocene to the ferrocenium ion. The BTDs **6a–6h**, **7a–7c**, **8a–8c**, **9a**, and **9b** exhibit one reversible

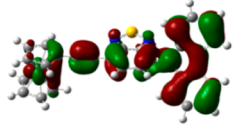
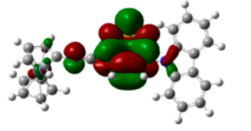
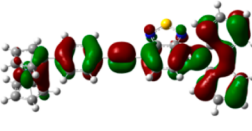
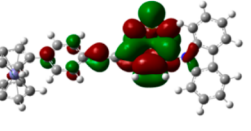
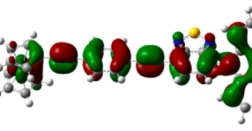
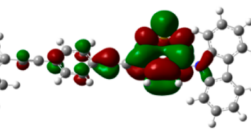
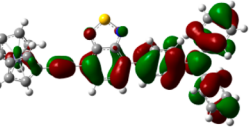
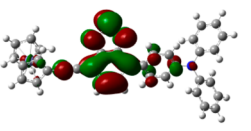
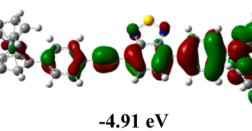
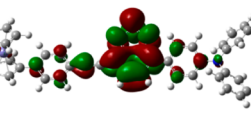
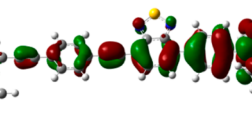
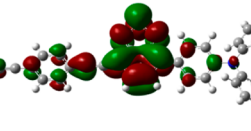
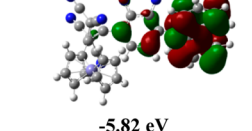
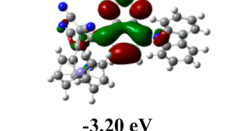
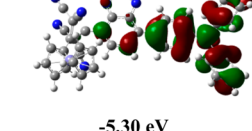
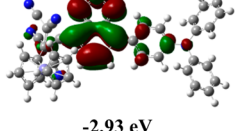
BTD	HOMO	LUMO	Calculated Band gap (eV)	Optical Band gap (eV) ^a
7a	 -5.30 eV	 -2.61 eV	2.69	2.18
7b	 -5.27 eV	 -2.65 eV	2.62	2.28
7c	 -5.28 eV	 -2.70 eV	2.57	2.30
8a	 -4.92 eV	 -2.40 eV	2.52	2.16
8b	 -4.91 eV	 -2.43 eV	2.48	2.25
8c	 -4.93 eV	 -2.47 eV	2.46	2.27
9a	 -5.82 eV	 -3.20 eV	2.62	1.98
9b	 -5.30 eV	 -2.93 eV	2.37	1.73

Figure 5. HOMO and LUMO frontier orbitals of unsymmetrical benzothiadiazoles **7a–7c**, **8a–8c**, **9a**, and **9b** at the B3LYP/6-31G** level for C, N, S, and H, and the Lanl2DZ level for Fe. (^a) Determined from the onset wavelength of the UV–vis absorption.

reduction wave in the region of -1.61 to -2.15 V attributed to the acceptor benzothiadiazole unit.^{7,8,12}

The trend in the oxidation potential of the ferrocenyl moiety in the BTDs **6a–6h** follows the order **6h** > **6c** > **6b** > **6d** > **6a** > **6g** > **6e** > **6f**, whereas the BTDs **7a–7c**, **8a–8c**, **9a**, and **9b** follow the order **9b** > **9a** > **7a** > **7c** > **7b** > **8a** > **8c** > **8b**. The ferrocenyl

moieties in the BTDs exhibit higher oxidation potentials compared to free ferrocene ($E^\circ = 0.00$ V, as recommended by IUPAC), confirming the strong electronic communication between the ferrocene unit and the BTD core.^{8,17} 1,1,4,4-Tetracyanobuta-1,3-diene (TCBD) is a strong electron-withdrawing group, which results in harder oxidation of the ferrocene unit.¹⁸

Table 2. Electrochemical Data of Unsymmetrical BTDs 6a–6h, 7a–7c, 8a–8c, 9a, and 9b

compound	electrochemical data ^a		compound	electrochemical data ^a	
	E_{ox} (V) ^b	E_{red} (V) ^b		E_{ox} (V) ^b	E_{red} (V) ^b
ferrocene	0.00	-	ferrocene	0.00	-
6a	0.12	-1.69	7a	0.10, 0.60, 0.82	-1.73
6b	0.13	-1.61	7b	0.04, 0.58, 0.80	-1.69
6c	0.14	-1.62	7c	0.10, 0.59, 0.82	-1.68
6d	0.13	-1.67	8a	0.13, 0.54	-1.82
6e	0.11	-1.66	8b	0.02, 0.52	-1.78
6f	0.11	-1.64	8c	0.11, 0.51	-1.76
6g	0.12	-1.66	9a	0.42, 0.62, 0.82	-0.83, -1.19, -2.08
6h	0.52, 0.95	-1.69	9b	0.41, 0.58	-0.85, -1.29, -2.15

^aRecorded by cyclic voltammetry, in 0.1 M solution of TBAPF₆ in DCM at 100 mV s⁻¹ scan rate, vs Fc/Fc⁺ at 25 °C. ^bFor the irreversible redox process, the peak potential is quoted.

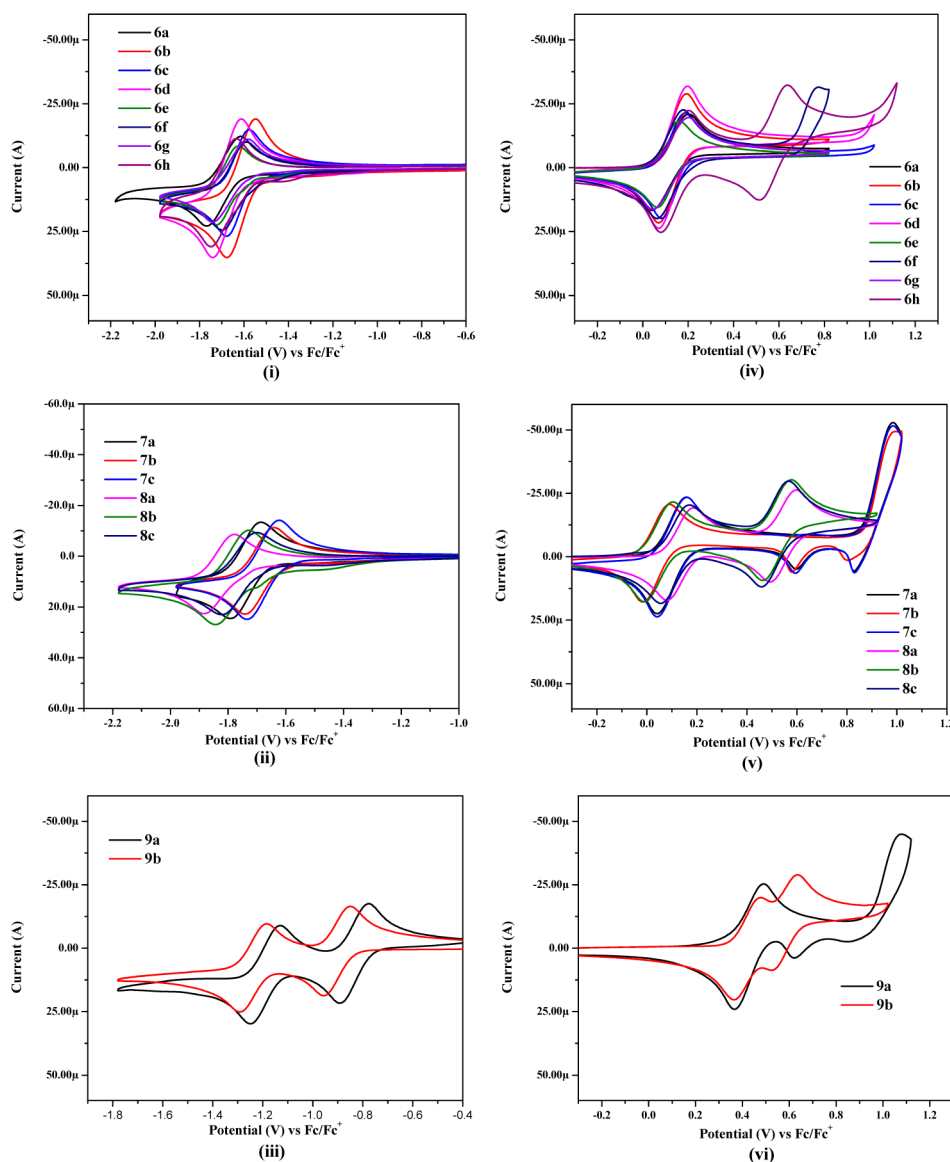


Figure 6. Cyclic voltammograms of unsymmetrical benzothiadiazoles 6a–6h, 7a–7c, 8a–8c, 9a, and 9b representing the reduction wave (i–iii), and the oxidation wave (iv–vi) at 0.01 M concentration in 0.1 M TBAPF₆ in dichloromethane recorded at a scan rate of 100 mV s⁻¹.

In addition to the ferrocene oxidation wave, a quasi-reversible oxidation wave due to the triphenylamine unit in BTDs 6h, 8a–8c, and 9b is observed in the region of 0.51–0.58 V.¹⁹ The BTDs 7a–7c and 9a exhibit two irreversible

oxidation waves in the region of 0.58–1.82 V attributed to the carbazole unit.²⁰

The reduction potential for the BTDs 6a–6h, 7a–7c, and 8a–8c shows less negative values compared to 2,1,3-benzothiadiazole

1 (−1.98 V vs Fc/Fc⁺ in DCM), indicating that the BTD rings in these ferrocenyl-substituted compounds are easier to reduce than unsubstituted BTD.^{7,8,21} The BTDs **9a** and **9b** exhibit two irreversible reduction waves in the region of −0.83 to −1.29 V attributed to the successive one-electron reductions of the dicyanovinyl (DCV) groups of the TCBD π -linker.²² The third reduction wave in BTDs **9a** and **9b** is assigned to the BTD unit and was observed at −2.08 and −2.15 V, respectively.

X-ray Analysis. The single crystal of the unsymmetrical BTDs **6c**, **6g**, **7a**, and **7b** were obtained via slow diffusion of ethanol into the chloroform solution at room temperature. The BTDs **6c** and **7a** crystallize in the monoclinic space group $P2_1/c$, whereas the BTD **6g** crystallizes in the monoclinic space group $P2_1/n$. The BTD **7b** crystallizes in the triclinic space group $P\bar{1}$. Figure 7 shows the single-crystal X-ray structure of **6c**, **6g**, **7a**, and **7b**.

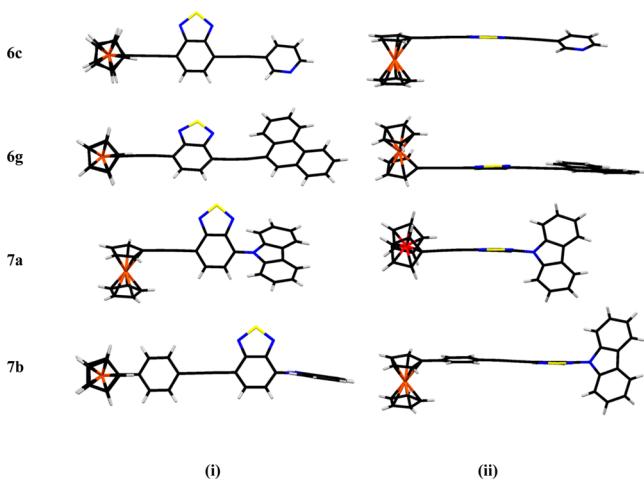


Figure 7. Single-crystal X-ray structure of ferrocenyl BTDs **6c**, **6g**, **7a**, and **7b**: (i) front view and (ii) side view. Solvent molecule (chloroform) is omitted from **7a** for clarity.

The BTD core shows a planar structure in the unsymmetrical BTDs **6c**, **6g**, **7a**, and **7b**. The cyclopentadienyl rings of the ferrocenyl moiety shows an eclipsed skew conformation in BTD **6c**, and an eclipsed conformation in BTDs **6g**, **7a**, and **7b**. The dihedral angle between the planes containing the BTD core and the cyclopentadienyl ring of ferrocene units was found to be 9.44° in **6c**, 41.06° in **6g**, 70.66° in **7a**, and 24.35° in **7b**. The important bond lengths and bond angles are listed in Table S2 (see the Supporting Information for details).

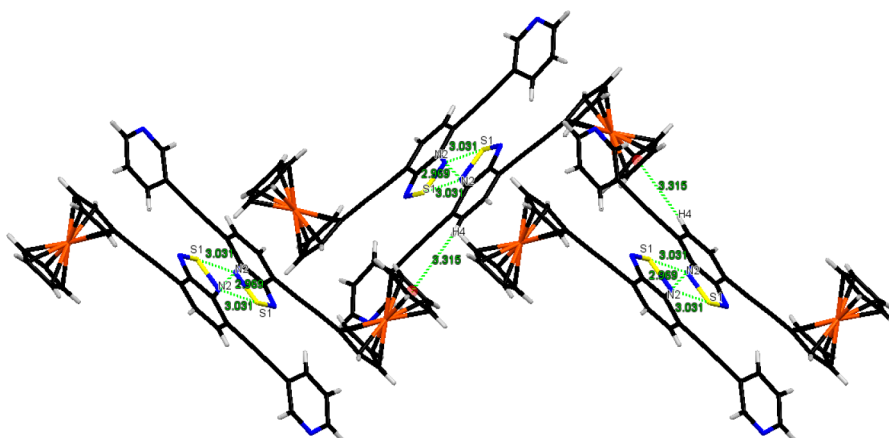


Figure 8. Packing diagram of ferrocenyl BTD **6c** forming a 2D zigzag chain along the *a* axis.

The packing diagram of BTD **6c** exhibits short S1...N2 (3.031(2) Å), and N2...N2 (2.969(5) Å) interheteroatom contacts between the BTD rings, which leads to the formation of dimers in head-to-head fashion.^{4a,8,23} The dimer units are interlinked through C-H... π interaction C4H4...C21-C25 (3.315(2) Å) to form a 2D zigzag chain (Figure 8).

The packing diagram of BTD **6g** exhibits short S1...N2 (3.124(5) Å) interheteroatom contacts between the BTD rings, resulting in the formation of dimers in head-to-head fashion.^{4a,8,23} The dimer units are interlinked through C-H... π interaction C21H21...C30-C34 (3.011(3) Å) to form a 2D zigzag chain (Figure 9).

The packing diagram of **7a** shows π ... π stacking interaction C7-C12...C1-C6 (3.817(2) Å) between the carbazole and the BTD units, which leads to the formation of a 1D polymeric chain. These chains are interlinked in *anti* fashion via intermolecular C-H... π interaction C15H15...C7-C12 (3.410(3) Å) to form a 2D sheetlike structure (Figure 10).

The packing diagram of BTD **7b** exhibits short S2...N2 (3.263(5) Å) interheteroatom contacts between the BTD rings, which leads to the formation of dimers in head-to-head fashion.^{4a,8,23} These dimers show π ... π stacking interaction C21-C26...C21-C26 (3.500(2) Å) between two adjacent carbazole units of the dimer. The dimer units are interlinked through C-H... π interaction C32H32...C15-C20 (2.893(4) Å) to form a 1D polymeric chain (Figure 11).

CONCLUSION

In summary, a series of aryl-substituted unsymmetrical benzothiadiazole derivatives were designed and synthesized by the Pd-catalyzed Sonogashira cross-coupling reaction. The photophysical and electrochemical properties show strong electronic communication. The enhancement of conjugation via a π -bridge resulted in the red shift of the absorption bands in BTDs **7a–7c**, **8a–8c**, **9a**, and **9b**. The incorporation of the 1,1,4,4-tetracyanobuta-1,3-diene group in benzothiadiazoles results in enhanced thermal stability. Our results provide the rationale to design low-band-gap materials for various optoelectronic applications. The detailed nonlinear optical characterizations of these ferrocenyl-substituted unsymmetrical BTDs are currently ongoing in our laboratory.

EXPERIMENTAL DETAILS

Chemicals were used as received unless otherwise indicated. All oxygen- or moisture-sensitive reactions were performed under a nitrogen/argon

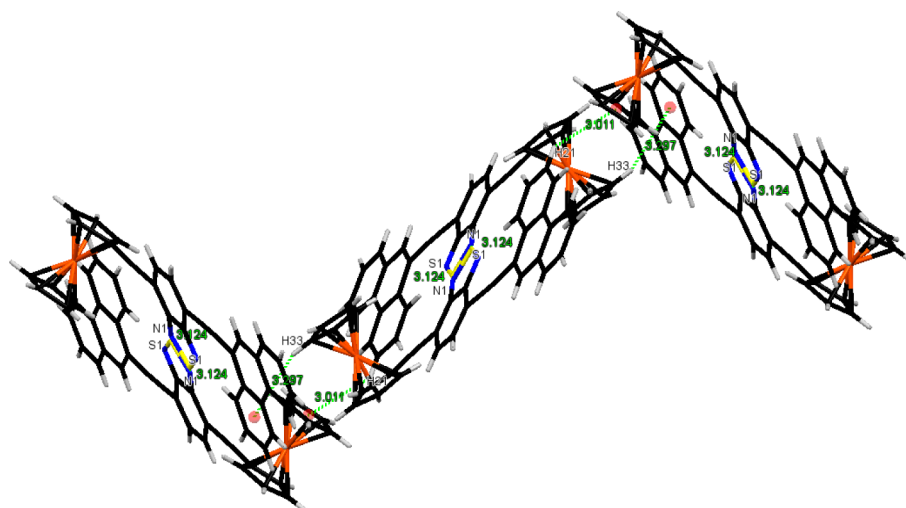


Figure 9. Packing diagram of ferrocenyl BTD **6g** forming a 2D zigzag chain along the *a* axis.

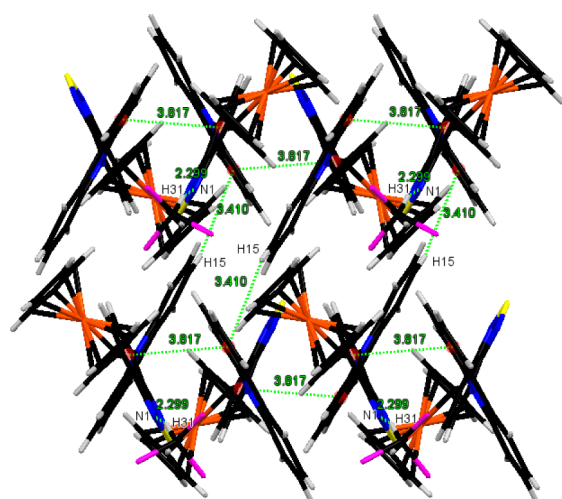


Figure 10. Packing diagram of ferrocenyl BTD **7a** forming a 2D sheet along the *a* axis.

atmosphere using standard Schlenk methods. Triethylamine (TEA) was received from a commercial source and distilled on KOH prior to use. ^1H NMR spectra were recorded using a 400 MHz spectrometer. Chemical shifts are reported in delta (δ) units, expressed in parts per million (ppm) downfield from tetramethylsilane using residual protonated solvent as an internal standard (CDCl_3 , 7.26 ppm; $(\text{CD}_3)_2\text{CO}$, 2.05). ^{13}C NMR spectra were recorded using a 100 MHz

spectrometer. Chemical shifts are reported in delta (δ) units, expressed in parts per million (ppm) downfield from tetramethylsilane using the solvent as an internal standard (CDCl_3 , 77.0 ppm; $(\text{CD}_3)_2\text{CO}$, 29.8; $\text{DMSO}-d_6$, 39.5 ppm). The ^1H NMR splitting patterns have been described as “s, singlet; bs, broad singlet; d, doublet; t, triplet; dd, doublet of doublets; dt, doublet of triplets; and m, multiplet”. UV–visible absorption spectra of all compounds were recorded in DCM. Cyclic voltamograms (CVs) were recorded on an electrochemical analyzer using glassy carbon as the working electrode, Pt wire as the counter electrode, and a saturated calomel electrode (SCE) as the reference electrode. The scan rate was 100 mV s^{-1} for CV. A solution of tetrabutylammoniumhexafluorophosphate (TBAPF_6) in CH_2Cl_2 (0.1 M) was employed as the supporting electrolyte. DCM was freshly distilled from CaH_2 prior to use. All potentials were experimentally referenced against the saturated calomel electrode couple but were then manipulated to be referenced against Fc/Fc^+ as recommended by IUPAC.²⁴ Under our conditions, the Fc/Fc^+ couple exhibited $E^\circ = 0.38\text{ V}$ versus SCE. HRMS was recorded on a TOF-Q mass spectrometer. The density functional theory (DFT) calculations were carried out at the B3LYP/6-31G** level for C, N, S, and H, and the LanL2DZ level for Fe in the Gaussian 09 program.²⁵

General Procedure for the Preparation of BTDs 6a–6c by Sonogashira Coupling Reaction. To a stirred solution of the respective aryl alkyne (**10a–10h**) (0.37 mmol), and ferrocenyl bromo-BTD **3a** (0.34 mmol) in THF, and TEA (1:1, v/v) were added $\text{PdCl}_2(\text{PPh}_3)_2$ (10 mg, 0.014 mmol) and CuI (2 mg, 0.01 mmol) under an argon flow at room temperature. The reaction mixture was stirred for 15–24 h at 60°C , and then cooled to room temperature. The solvent was then evaporated under reduced pressure, and the mixture was purified by SiO_2 chromatography with DCM/hexane (2:3, v/v),

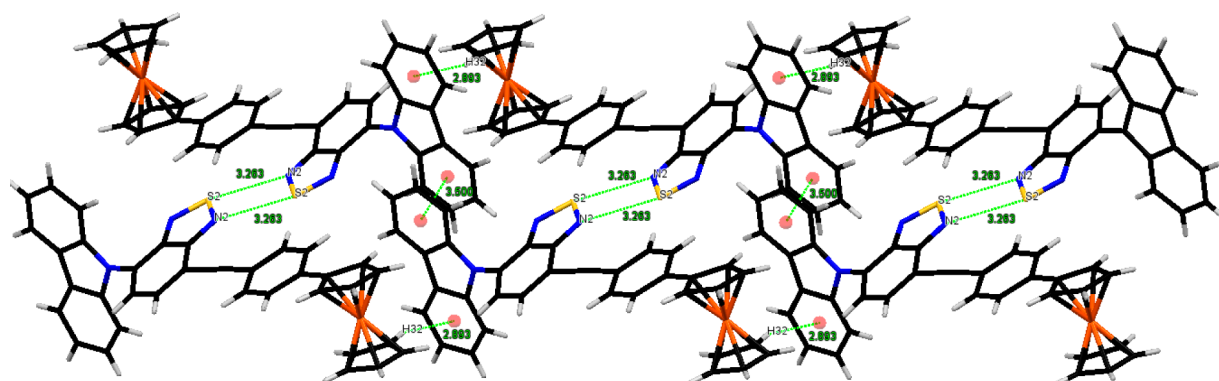


Figure 11. Packing diagram of ferrocenyl BTD **7b** forming a 2D sheet along the *b* axis.

followed by recrystallization in chloroform:ethanol (1:1) to obtain **6a–6h** as colored solids.

Compound 6a: Deep-red solid (73 mg, Yield: 48%): mp 200.0–201.5 °C; $^1\text{H NMR}$ (400 MHz, $(\text{CD}_3)_2\text{CO}$, δ in ppm) 7.89 (d, 1H, $J = 7.3$ Hz), 7.84 (d, 1H, $J = 7.3$ Hz), 4.65 (t, 2H, $J = 1.8$ Hz), 4.40 (t, 2H, $J = 1.8$ Hz), 4.32 (s, 5H); $^{13}\text{C NMR}$ (100 MHz, DMSO- d_6 , δ in ppm) 153.7, 134.3, 132.8, 131.8, 131.5, 131.4, 128.7, 128.5, 121.7, 117.1, 115.2, 96.3, 85.6, 81.8, 71.4, 69.9, 69.5, 63.6; HRMS (ESI-TOF) m/z calcd for $\text{C}_{26}\text{H}_{16}\text{FeN}_2\text{S}$ 444.0378 $[\text{M}]^+$, found 444.0376 $[\text{M}]^+$; UV/vis (DCM) λ_{max} (ϵ $[\text{M}^{-1} \text{cm}^{-1}]$) 406 (32791), 509 (9324).

Compound 6b: Deep-red solid (76 mg, Yield: 50%): mp 225.5–226.5 °C; $^1\text{H NMR}$ (400 MHz, $(\text{CD}_3)_2\text{CO}$, δ in ppm) 7.97 (d, 1H, $J = 7.5$ Hz), 7.92–7.86 (m, 3H), 7.73 (dt, 1H, $J = 7.8$ Hz, $J = 1$ Hz), 7.46–7.42 (m, 1H), 4.65 (t, 2H, $J = 2.0$ Hz), 4.41 (t, 2H, $J = 2.0$ Hz), 4.32 (s, 5H); $^{13}\text{C NMR}$ (100 MHz, DMSO- d_6 , δ in ppm) 150.4, 145.9, 139.0, 136.9, 132.1, 131.9, 127.6, 124.2, 111.1, 108.4, 106.2, 101.9, 98.0, 92.7, 82.3, 71.5, 70.0, 69.7, 63.3; HRMS (ESI-TOF) m/z calcd for $\text{C}_{25}\text{H}_{15}\text{FeN}_3\text{S}$ 446.0409 $[\text{M} + \text{H}]^+$, found 446.0407 $[\text{M} + \text{H}]^+$; UV/vis (DCM) λ_{max} (ϵ $[\text{M}^{-1} \text{cm}^{-1}]$) 399 (85328), 511 (22404).

Compound 6c: Deep-red solid (91 mg, Yield: 60%): mp > 300 °C; $^1\text{H NMR}$ (400 MHz, CDCl_3 , δ in ppm) 8.90 (bs, 1H), 8.62–8.60 (m, 1H), 7.95 (dt, 1H, $J = 8$ Hz, $J = 1.8$ Hz), 7.80 (d, 1H, $J = 7.6$ Hz), 7.75 (d, 1H, $J = 7.3$), 4.66 (t, 2H, $J = 1.8$ Hz), 4.34 (t, 2H, $J = 2.0$ Hz), 4.31 (s, 5H); $^{13}\text{C NMR}$ (100 MHz, DMSO- d_6 , δ in ppm) 153.6, 138.6, 135.9, 133.4, 133.1, 132.0, 131.8, 117.6, 114.4, 113.7, 113.2, 108.0, 104.5, 100.8, 95.3, 71.4, 69.9, 63.2; HRMS (ESI-TOF) m/z calcd for $\text{C}_{25}\text{H}_{15}\text{FeN}_3\text{S}$ 446.0363 $[\text{M} + \text{H}]^+$, found 446.0360 $[\text{M} + \text{H}]^+$; UV/vis (DCM) λ_{max} (ϵ $[\text{M}^{-1} \text{cm}^{-1}]$) 402 (85328), 515 (20963).

Compound 6d: Deep-red solid (124 mg, Yield: 70%): mp 191.5–192.5 °C; $^1\text{H NMR}$ (400 MHz, $(\text{CD}_3)_2\text{CO}$, δ in ppm) 7.92 (d, 1H, $J = 7.5$ Hz), 7.85 (d, 1H, $J = 7.5$ Hz), 7.81–7.73 (m, 6H), 7.52–7.48 (m, 2H), 7.42–7.39 (m, 1H), 4.65 (t, 2H, $J = 2.0$ Hz), 4.40 (t, 2H, $J = 1.8$ Hz), 4.32 (s, 5H); $^{13}\text{C NMR}$ (100 MHz, CDCl_3 , δ in ppm) 154.25, 154.22, 141.5, 140.0, 132.4, 132.2, 131.7, 128.7, 127.6, 126.9, 121.3, 117.7, 116.2, 97.8, 97.0, 86.0, 81.9, 72.8, 71.6, 70.9, 65.8; HRMS (ESI-TOF) m/z calcd for $\text{C}_{32}\text{H}_{20}\text{FeN}_2\text{S}$ 520.0692 $[\text{M}]^+$, found 520.0692 $[\text{M}]^+$; UV/vis (DCM) λ_{max} (ϵ $[\text{M}^{-1} \text{cm}^{-1}]$) 413 (55533), 512 (14750).

Compound 6e: Deep-red solid (117 mg, Yield: 70%): mp 199.0–200.5 °C; $^1\text{H NMR}$ (400 MHz, $(\text{CD}_3)_2\text{CO}$, δ in ppm) 8.76 (d, 1H, $J = 8.3$ Hz), 8.06–8.02 (m, 3H), 7.94–7.88 (m, 2H), 7.77–7.73 (m, 1H), 7.67–7.58 (m, 2H), 4.66 (t, 2H, $J = 1.8$ Hz), 4.41 (t, 2H, $J = 1.8$ Hz), 4.33 (s, 5H); $^{13}\text{C NMR}$ (100 MHz, CDCl_3 , δ in ppm) 154.0, 153.7, 132.7, 132.6, 131.7, 131.2, 130.1, 129.0, 127.7, 126.6, 126.0, 125.7, 124.7, 119.6, 117.4, 115.7, 97.2, 94.7, 90.0, 81.4, 71.5, 69.9, 69.4, 63.9; HRMS (ESI-TOF) m/z calcd for $\text{C}_{30}\text{H}_{18}\text{FeN}_2\text{S}$ 494.0535 $[\text{M}]^+$, found 494.0533 $[\text{M}]^+$; UV/vis (DCM) λ_{max} (ϵ $[\text{M}^{-1} \text{cm}^{-1}]$) 421 (54400), 521 (sh).

Compound 6f: Deep-red solid (120 mg, Yield: 65%): mp 192.5–193.8 °C; $^1\text{H NMR}$ (400 MHz, $(\text{CD}_3)_2\text{CO}$, δ in ppm) 8.99–8.96 (m, 2H), 8.72 (s, 1H), 8.21–8.17 (m, 2H), 7.94 (d, 1H, $J = 7.5$ Hz), 7.79–7.75 (m, 2H), 7.66–7.62 (m, 2H), 4.68 (t, 2H, $J = 1.8$ Hz), 4.42 (t, 2H, $J = 1.8$ Hz), 4.34 (s, 5H); $^{13}\text{C NMR}$ (100 MHz, CDCl_3 , δ in ppm) 154.4, 154.2, 132.6, 131.7, 131.6, 130.9, 128.5, 127.3, 127.2, 126.8, 126.6, 125.6, 123.0, 117.6, 116.4, 116.3, 97.6, 96.8, 94.2, 81.9, 71.9, 70.3, 69.7, 63.8; HRMS (ESI-TOF) m/z calcd for $\text{C}_{34}\text{H}_{20}\text{FeN}_2\text{S}$ 544.0692 $[\text{M}]^+$, found 544.0694 $[\text{M}]^+$; UV/vis (DCM) λ_{max} (ϵ $[\text{M}^{-1} \text{cm}^{-1}]$) 465 (67550).

Compound 6g: Deep-red solid (74 mg, Yield: 40%): mp 201.5–202.4 °C; $^1\text{H NMR}$ (400 MHz, $(\text{CD}_3)_2\text{CO}$, δ in ppm) 8.93–8.86 (m, 3H), 8.32 (s, 1H), 8.10–8.05 (m, 2H), 7.91 (d, 1H, $J = 7.3$), 7.88–7.76 (m, 3H), 7.74–7.71 (m, 1H), 4.67 (t, 2H, $J = 2.0$ Hz), 4.42 (t, 2H, $J = 2.0$ Hz), 4.34 (s, 5H); $^{13}\text{C NMR}$ (100 MHz, CDCl_3 , δ in ppm) 154.3, 154.1, 140.0, 132.2, 132.1, 131.5, 130.7, 130.6, 130.2, 129.7, 128.4, 127.6, 127.1, 127.0, 126.8, 122.5, 122.3, 118.8, 117.7, 115.9, 97.6, 95.2, 89.8, 81.7, 71.9, 70.3, 69.6, 63.5; HRMS (ESI-TOF) m/z calcd for $\text{C}_{34}\text{H}_{20}\text{FeN}_2\text{S}$ 544.0692 $[\text{M}]^+$, found 544.0708 $[\text{M}]^+$; UV/vis (DCM) λ_{max} (ϵ $[\text{M}^{-1} \text{cm}^{-1}]$) 423 (58074), 514 (sh).

Compound 6h: Deep-red solid (114 mg, Yield: 55%): mp 182.0–183.0 °C; $^1\text{H NMR}$ (400 MHz, $(\text{CD}_3)_2\text{CO}$, δ in ppm) 7.85–7.80 (m, 2H), 7.55–7.51 (m, 2H), 7.39–7.35 (m, 2H), 7.17–7.13 (m, 2H), 7.03–7.00 (m, 2H), 4.64 (t, 2H, $J = 1.8$ Hz), 4.39 (t, 2H, $J = 2.0$ Hz), 4.32 (s, 5H); $^{13}\text{C NMR}$ (100 MHz, CDCl_3 , δ in ppm) 154.0, 153.9, 148.1,

146.5, 132.4, 131.6, 131.4, 129.0, 124.8, 123.4, 121.2, 116.9, 116.3, 114.6, 97.4, 97.0, 84.6, 81.5, 71.5, 69.9, 69.1, 63.9; HRMS (ESI-TOF) m/z calcd for $\text{C}_{38}\text{H}_{25}\text{FeN}_3\text{S}$ 611.1114 $[\text{M}]^+$, found 611.1115 $[\text{M}]^+$; UV/vis (DCM) λ_{max} (ϵ $[\text{M}^{-1} \text{cm}^{-1}]$) 460 (58729).

General Procedure for the Preparation of BTDs 7a–7c and 8a–8c by Sonogashira Coupling Reaction. To a stirred solution of the respective alkynyl ferrocene (0.37 mmol), and bromo-BTDs **4a/5a** (0.34 mmol) in THF, and TEA (1:1, v/v) were added $\text{PdCl}_2(\text{PPh}_3)_2$ (10 mg, 0.014 mmol) and CuI (2 mg, 0.01 mmol) under an argon flow at room temperature. The reaction mixture was stirred for 12 h at 60 °C, and then cooled to room temperature. The solvent was then evaporated under reduced pressure, and the mixture was purified by SiO_2 chromatography with DCM/hexane (2:3, v/v), followed by recrystallization in chloroform:ethanol (1:1) to obtain **7a–7c** and **8a–8c** as colored solids.

Compound 7a: Red solid (121 mg, Yield: 70%): mp 185.5–186.5 °C; $^1\text{H NMR}$ (400 MHz, $(\text{CD}_3)_2\text{CO}$, δ in ppm) 8.26–8.24 (m, 2H), 8.09 (d, 1H, $J = 7.5$ Hz), 7.99 (d, 1H, $J = 7.5$ Hz), 7.41–7.37 (m, 2H), 7.33–7.28 (m, 4H), 4.69 (t, 2H, $J = 1.8$ Hz), 4.42 (t, 2H, $J = 2.0$ Hz), 4.35 (s, 5H); $^{13}\text{C NMR}$ (100 MHz, CDCl_3 , δ in ppm) 155.9, 151.2, 140.9, 131.9, 129.4, 127.7, 125.9, 123.9, 120.6, 120.4, 117.5, 110.3, 97.2, 81.46, 72.7, 71.3, 70.6, 65.3; HRMS (ESI-TOF) m/z calcd for $\text{C}_{30}\text{H}_{19}\text{FeN}_3\text{S}$ 509.0644 $[\text{M}]^+$, found 509.0666 $[\text{M}]^+$; UV/vis (DCM) λ_{max} (ϵ $[\text{M}^{-1} \text{cm}^{-1}]$) 443 (35138), 520 (sh).

Compound 7b: Orange solid (129 mg, Yield: 65%): mp 198.0–199.5 °C; $^1\text{H NMR}$ (400 MHz, $(\text{CD}_3)_2\text{CO}$, δ in ppm) 8.27–8.24 (m, 2H), 8.18 (d, 1H, $J = 7.5$ Hz), 8.04 (d, 1H, $J = 7.5$ Hz), 7.70–7.68 (m, 2H), 7.64–7.62 (m, 2H), 7.42–7.37 (m, 2H), 7.34–7.30 (m, 4H), 4.86 (t, 2H, $J = 1.8$ Hz), 4.42 (t, 2H, $J = 1.8$ Hz), 4.07 (s, 5H); $^{13}\text{C NMR}$ (100 MHz, DMSO- d_6 , δ in ppm) 155.4, 150.7, 141.1, 140.5, 133.1, 131.7, 129.2, 128.2, 126.1, 123.1, 120.5, 120.4, 118.7, 115.8, 110.8, 96.6, 85.6, 83.3, 69.6, 69.64, 66.6; HRMS (ESI-TOF) m/z calcd for $\text{C}_{36}\text{H}_{23}\text{FeN}_3\text{S}$ 585.0957 $[\text{M}]^+$, found 585.0952 $[\text{M}]^+$; UV/vis (DCM) λ_{max} (ϵ $[\text{M}^{-1} \text{cm}^{-1}]$) 453 (47855).

Compound 7c: Orange solid (124 mg, Yield: 60%): mp 220.5–221.2 °C; $^1\text{H NMR}$ (400 MHz, $(\text{CD}_3)_2\text{CO}$, δ in ppm) 8.27–8.26 (m, 2H), 8.20 (d, 2H, $J = 7.5$ Hz), 8.06 (d, 2H, $J = 7.5$ Hz), 7.73–7.71 (m, 2H), 7.61–7.59 (m, 2H), 7.42–7.38 (m, 2H), 7.34–7.30 (m, 2H), 4.56 (t, 2H, $J = 1.8$ Hz), 4.34 (t, 2H, $J = 2.0$ Hz), 4.28 (s, 5H); $^{13}\text{C NMR}$ (100 MHz, DMSO- d_6 , δ in ppm) 155.2, 150.5, 140.3, 133.1, 131.6, 131.2, 129.4, 127.9, 125.9, 124.0, 123.0, 120.9, 120.3, 120.1, 115.3, 110.5, 95.5, 91.4, 86.9, 84.9, 71.1, 69.7, 69.0, 63.8; HRMS (ESI-TOF) m/z calcd for $\text{C}_{38}\text{H}_{23}\text{FeN}_3\text{S}$ 609.0957 $[\text{M}]^+$, found 609.0956 $[\text{M}]^+$; UV/vis (DCM) λ_{max} (ϵ $[\text{M}^{-1} \text{cm}^{-1}]$) 454 (62777).

Compound 8a: Red solid (120 mg, Yield: 68%): mp 180.5–181.6 °C; $^1\text{H NMR}$ (400 MHz, $(\text{CD}_3)_2\text{CO}$, δ in ppm) 8.03–8.01 (m, 2H), 7.89 (d, 1H, $J = 7.5$ Hz), 7.84 (d, 1H, $J = 7.5$ Hz), 7.38–7.34 (m, 4H), 7.18–7.10 (m, 8H), 4.63 (t, 2H, $J = 1.8$ Hz), 4.38 (t, 2H, $J = 1.8$ Hz), 4.32 (s, 5H); $^{13}\text{C NMR}$ (100 MHz, CDCl_3 , δ in ppm) 155.3, 153.1, 148.3, 147.2, 133.2, 132.4, 130.3, 129.8, 129.3, 126.7, 124.9, 123.3, 122.6, 115.7, 95.5, 81.9, 71.9, 70.3, 69.4, 64.8; HRMS (ESI-TOF) m/z calcd for $\text{C}_{36}\text{H}_{23}\text{FeN}_3\text{S}$ 587.1114 $[\text{M}]^+$, found 587.1114 $[\text{M}]^+$; UV/vis (DCM) λ_{max} (ϵ $[\text{M}^{-1} \text{cm}^{-1}]$) 458 (37842).

Compound 8b: Orange solid (140 mg, Yield: 62%): mp 202.0–203.5 °C; $^1\text{H NMR}$ (400 MHz, $(\text{CD}_3)_2\text{CO}$, δ in ppm) 8.04 (d, 2H, $J = 9.0$ Hz), 7.98 (d, 1H, $J = 7.5$ Hz), 7.89 (d, 1H, $J = 7.5$ Hz), 7.65 (d, 2H, $J = 8.5$ Hz), 7.58 (d, 2H, $J = 8.0$ Hz), 7.38–7.34 (m, 4H), 7.18–7.10 (m, 8H), 4.84 (t, 2H, $J = 2.0$ Hz), 4.41 (t, 2H, $J = 2.0$ Hz), 4.06 (s, 5H); $^{13}\text{C NMR}$ (100 MHz, CDCl_3 , δ in ppm) 155.4, 153.1, 148.3, 147.3, 140.5, 133.9, 132.9, 131.8, 130.2, 130.0, 129.3, 126.6, 125.9, 125.0, 123.4, 122.6, 119.9, 115.2, 96.2, 85.8, 70.6, 70.2, 67.1; HRMS (ESI-TOF) m/z calcd for $\text{C}_{42}\text{H}_{29}\text{FeN}_3\text{S}$ 663.1427 $[\text{M}]^+$, found 663.1426 $[\text{M}]^+$; UV/vis (DCM) λ_{max} (ϵ $[\text{M}^{-1} \text{cm}^{-1}]$) 466 (51474).

Compound 8c: Orange solid (152 mg, Yield: 65%): mp 189.5–190.5 °C; $^1\text{H NMR}$ (400 MHz, $(\text{CD}_3)_2\text{CO}$, δ in ppm) 8.04 (d, 2H, $J = 9$ Hz), 8.00 (d, 1H, $J = 7.28$ Hz), 7.90 (d, 1H, $J = 7.28$ Hz), 7.67 (d, 2H, $J = 8.80$ Hz), 7.57 (d, 2H, $J = 8.52$ Hz), 7.39–7.35 (m, 4H), 7.18–7.11 (m, 8H), 4.55 (t, 2H, $J = 1.8$ Hz), 4.33 (t, 2H, $J = 2.0$ Hz), 4.27 (s, 5H); $^{13}\text{C NMR}$ (100 MHz, CDCl_3 , δ in ppm) 154.9, 152.5, 147.9, 146.7, 145.3, 141.8, 133.8, 132.8, 131.3, 130.7, 129.5, 128.9, 126.0, 124.4, 123.0, 121.9, 114.0, 109.7, 96.3, 94.3, 93.2, 87.1,

73.4, 70.8, 69.4, 64.9; HRMS (ESI-TOF) m/z calcd for $C_{44}H_{29}FeN_3S$ 687.1427 $[M]^+$, found 687.1426 $[M]^+$; UV/vis (DCM) λ_{max} (ϵ [$M^{-1}cm^{-1}$]) 467 (84788).

General Procedure for the Preparation of BTDs 9a and 9b. TCNE (77 mg, 0.60 mmol) was added to a solution of 7a/8a (0.30 mmol) in DCM (60 mL) at room temperature. The mixture was refluxed at 40 °C for 15 h. The solvent was removed in vacuo, and the product was purified by SiO_2 chromatography with DCM as the eluent to yield 9a/9b as a dark colored solid.

Compound 9a: Purple solid (134 mg, Yield: 70%); mp 279.5–280.5 °C; 1H NMR (400 MHz, $(CD_3)_2CO$, δ in ppm) 8.76 (d, 1H, $J = 7.5$ Hz), 8.31 (d, 2H, $J = 7.3$ Hz), 7.40–7.29 (m, 4H), 7.24–7.12 (m, 2H), 5.46–5.45 (m, 1H), 5.07–5.05 (m, 1H), 5.01–5.00 (m, 1H), 4.92–4.91 (m, 1H), 4.39 (s, 5H); ^{13}C NMR (100 MHz, $CDCl_3$, δ in ppm) 171.0, 160.9, 152.1, 150.5, 140.0, 135.2, 131.9, 126.0, 125.5, 124.3, 124.2, 122.8, 121.3, 120.2, 113.8, 111.4, 110.7, 110.5, 90.5, 79.3, 75.9, 74.8, 74.2, 73.0, 72.4, 70.7, 65.5; HRMS (ESI-TOF) m/z calcd for $C_{36}H_{19}FeN_3S$ 637.0767 $[M]^+$, found 637.0774 $[M]^+$; UV/vis (DCM) λ_{max} (ϵ [$M^{-1}cm^{-1}$]) 502 (46178).

Compound 9b: Deep-green solid (172 mg, Yield: 80%); mp 222.5–223.5 °C; 1H NMR (400 MHz, $(CD_3)_2CO$, δ in ppm) 8.52 (d, 1H, $J = 7.8$ Hz), 8.10–8.07 (m, 3H), 7.40–7.36 (m, 4H), 7.19–7.10 (m, 8H), 5.40–5.38 (m, 1H), 5.00–4.99 (m, 1H), 4.89–4.87 (m, 1H), 4.85–4.83 (m, 1H), 4.35 (s, 5H); ^{13}C NMR (100 MHz, $CDCl_3$, δ in ppm) 171.3, 164.8, 161.5, 152.9, 151.4, 149.3, 146.4, 139.3, 132.0, 130.3, 129.2, 127.8, 125.3, 125.2, 125.1, 123.9, 121.8, 121.1, 111.7, 101.3, 89.0, 82.1, 79.2, 75.5, 74.5, 74.2, 72.7, 72.1, 70.6, 64.6; HRMS (ESI-TOF) m/z calcd for $C_{42}H_{25}FeN_3S$ 715.1237 $[M]^+$, found 715.1240 $[M]^+$; UV/vis (DCM) λ_{max} (ϵ [$M^{-1}cm^{-1}$]) 554 (61482).

ASSOCIATED CONTENT

Supporting Information

Characterization data for all the new compounds; copies of 1H , ^{13}C NMR, and HRMS spectra of new compounds; crystallographic information files (CIFs) for compounds 6c (CCDC: 959150), 6g (CCDC: 959151), 7a (CCDC: 959148), and 7b (CCDC: 959149); the DFT calculation data of all the new compounds; and the electrochemical data of compounds 9a and 9b. This material is available free of charge via the Internet at <http://pubs.acs.org>.

AUTHOR INFORMATION

Corresponding Author

*E-mail: rajneeshmisra@iiti.ac.in.

Notes

The authors declare no competing financial interest.

ACKNOWLEDGMENTS

R.M. thanks CSIR, and DST, New Delhi, for financial support. We are grateful to the Sophisticated Instrumentation Centre (SIC) Single Crystal X-Ray diffraction Facility, IIT Indore.

REFERENCES

- (1) (a) Sonar, P.; Singh, S. P.; Li, Y.; Soh, M. S.; Dodabalapur, A. *Adv. Mater.* **2010**, *22*, 5409–5413. (b) Kato, S.; Furuya, T.; Kobayashi, A.; Nitani, M.; Ie, Y.; Aso, Y.; Yoshihara, T.; Tobita, S.; Nakamura, Y. *J. Org. Chem.* **2012**, *77*, 7595–7606. (c) Omer, K. M.; Ku, S. Y.; Wong, K. T.; Bard, A. J. *J. Am. Chem. Soc.* **2009**, *131*, 10733–10741. (d) Li, Y.; Li, A.-Y.; Li, B.-X.; Huang, J.; Zhao, L.; Wang, B.-Z.; Li, J.-W.; Zhu, X.-H.; Peng, J.; Cao, Y.; Ma, D.-G.; Roncali, J. *Org. Lett.* **2009**, *11*, 5318–5321. (e) Wang, J.-L.; Tang, Z.-M.; Xiao, Q.; Ma, Y.; Pei, J. *Org. Lett.* **2009**, *11*, 863–866. (f) Kato, S.; Matsumoto, T.; Ishi-i, T.; Thiemann, T.; Shigeiwa, M.; Gorohmaru, H.; Maeda, S.; Yamashita, Y.; Mataka, S. *Chem. Commun.* **2004**, 2342–2343. (g) Neto, B. A. D.; Lapis, A. A. M.; Júnior, E. N. da S.; Dupont, J. *Eur. J. Org. Chem.* **2013**, 228–255. (h) Kato, S.; Matsumoto, T.; Shigeiwa, M.; Gorohmaru, H.; Maeda, S.; Ishi-i, T.; Mataka, S. *Chem.—Eur. J.* **2006**, *12*, 2303–2317. (i) Kobayashi, N.; Inagaki, S.; Nemykin, V. N.; Nonomura, T. *Angew. Chem., Int. Ed.* **2001**, *40*, 2710–2712. (j) Lindner, B. D.; Engelhart, J. U.; Märken, M.; Tverskoy, O.; Appleton, A. L.; Rominger, F.; Hardcastle, K. I.; Enders, M.; Bunz, U. H. F. *Chem.—Eur. J.* **2012**, *18*, 4627–4633. (k) Aviram, A.; Ratner, M. A. *Chem. Phys. Lett.* **1974**, *29*, 277–283. (2) (a) Wang, J.-L.; Xiao, Q.; Pei, J. *Org. Lett.* **2010**, *12*, 4164–4167. (b) Zhang, H.; Wan, X.; Xue, X.; Li, Y.; Yu, A.; Chen, Y. *Eur. J. Org. Chem.* **2010**, 1681–1687. (c) Bures, F.; Schweizer, W. B.; May, J. C.; Boudon, C.; Gisselbrecht, J.-P.; Gross, M.; Biaggio, I.; Diederich, F. *Chem.—Eur. J.* **2007**, *13*, 5378–5387. (3) (a) Tang, Z. M.; Lei, T.; Jiang, K. J.; Song, Y. L.; Pei, J. *Chem.—Asian J.* **2010**, *5*, 1911–1917. (b) Wu, Y.; Zhu, W. *Chem. Soc. Rev.* **2013**, *42*, 2039–2058. (4) (a) Chen, S.; Li, Y.; Yang, W.; Chen, N.; Liu, H.; Li, Y. *J. Phys. Chem. C* **2010**, *114*, 15109–15115. (b) Tambara, K.; Pantoş, G. D. *Annu. Rep. Prog. Chem., Sect. B: Org. Chem.* **2012**, *108*, 186–201. (c) Polander, L. E.; Pandey, L. S.; Barlow, S.; Tiwari, S. P.; Risko, C.; Kippelen, B.; Brédas, J.; Marder, S. R. *J. Phys. Chem. C* **2011**, *115*, 23149–23163. (d) Shi, C. J.; Yao, Y.; Yang, Y.; Pei, Q. B. *J. Am. Chem. Soc.* **2006**, *128*, 8980–8986. (e) Hou, Q.; Zhou, Q. M.; Zhang, Y.; Yang, W.; Yang, R. Q.; Cao, Y. *Macromolecules* **2004**, *37*, 6299–6305. (f) Zhu, Z.; Waller, D.; Gaudiana, R.; Morana, M.; Muhlbacher, D.; Scharber, M.; Brabec, C. *Macromolecules* **2007**, *40*, 1981–1986. (g) Thomas, K. R. J.; Lin, J. T.; Velusamy, M.; Tao, Y. T.; Chuen, C. H. *Adv. Funct. Mater.* **2004**, *14*, 83–90. (5) (a) Gautam, P.; Dhokale, B.; Shukla, V.; Singh, C. P.; Bindra, K. S.; Misra, R. *J. Photochem. Photobiol., A* **2012**, *239*, 24–27. (b) Jadhav, T.; Maragani, R.; Misra, R.; Sreeramulu, V.; Rao, D. N.; Mobin, S. M. *Dalton Trans.* **2013**, *42*, 4340–4342. (c) Maragani, R.; Thaksen, J.; Mobin, S. M.; Misra, R. *RSC Adv.* **2013**, *3*, 2889–2892. (6) (a) Gautam, P.; Dhokale, B.; Mobin, S. M.; Misra, R. *RSC Adv.* **2012**, *2*, 12105–12107. (b) Dhokale, B.; Gautam, P.; Mobin, S. M.; Misra, R. *Dalton Trans.* **2013**, *42*, 1512–1518. (c) Sharma, R.; Maragani, R.; Mobin, S. M.; Misra, R. *RSC Adv.* **2013**, *3*, 5785–5788. (7) Misra, R.; Gautam, P.; Sharma, R.; Mobin, S. M. *Tetrahedron Lett.* **2013**, *54*, 381–383. (8) Misra, R.; Gautam, P.; Jadhav, T.; Mobin, S. M. *J. Org. Chem.* **2013**, *78*, 4940–4948. (9) Wang, B.; Tsang, S.; Zhang, W.; Tao, Y.; Wong, M. S. *Chem. Commun.* **2011**, *47*, 9471–9473. (10) Karpicz, R.; Puzinas, S.; Krotkus, S.; Kazlauskas, K.; Jursenas, S.; Grazulevicius, J. V.; Grigalevicius, S.; Gulbinas, V. *J. Chem. Phys.* **2011**, *134*, 204508–204516. (11) Velusamy, M.; Justin Thomas, K. R.; Lin, J. T.; Hsu, Y.-C.; Ho, K.-C. *Org. Lett.* **2005**, *7*, 1899–1902. (12) Chen, S.; Li, Y.; Liu, C.; Yang, W.; Li, Y. *Eur. J. Org. Chem.* **2011**, *32*, 6445–6451. (13) (a) Wang, J. L.; Tang, Z. M.; Xiao, Q.; Ma, Y. G.; Pei, J. *Org. Lett.* **2008**, *10*, 4271–4274. (b) Zhang, H.; Wan, X.; Xue, X.; Li, Y.; Yu, A.; Chen, Y. *Eur. J. Org. Chem.* **2010**, 1681–1687. (c) Xu, E.; Zhong, H.; Du, J.; Zeng, D.; Ren, S.; Sun, J.; Fang, Q. *Dyes Pigm.* **2009**, *80*, 194–198. (d) Tao, Y.-M.; Li, H.-Y.; Xu, Q.-L.; Zhu, Y.-C.; Kang, L.-C.; Zheng, Y.-X.; Zuo, J.-L.; You, X.-Z. *Synth. Met.* **2011**, *161*, 718–723. (14) Vieira, A. A.; Cristiano, R.; Bortoluzzi, A. J.; Gallardo, H. J. *Mol. Struct.* **2008**, *875*, 364–371. (15) Ziessel, R.; Retailleau, P.; Elliott, K. J.; Harriman, A. *Chem.—Eur. J.* **2009**, *15*, 10369–10374. (16) (a) Watanabe, M.; Goto, K.; Fujitsuka, M.; Tojo, S.; Majima, T.; Shimmyozu, T. *Bull. Chem. Soc. Jpn.* **2010**, *83*, 1155–1161. (b) Xu, E.; Zhong, H.; Lai, H.; Zeng, D.; Zhang, J.; Zhu, W.; Fang, Q. *Macromol. Chem. Phys.* **2010**, *211*, 651–656. (17) (a) Maragani, R.; Jadhav, T.; Mobin, S. M.; Misra, R. *Tetrahedron* **2012**, *68*, 7302–7308. (b) Misra, R.; Kumar, R.; Chandrashekar, T. K.; Suresh, C. H.; Nag, A.; Goswami, D. *J. Am. Chem. Soc.* **2006**, *128*, 16083–16091. (18) Niu, S.; Ulrich, G.; Retailleau, P.; Ziessel, R. *Tetrahedron Lett.* **2011**, *52*, 4848–4853.

(19) (a) Lambert, C.; Gaschler, W.; Schmäzlin, E.; Meerholz, K.; Bräuchle, C. *J. Chem. Soc., Perkin Trans. 2* **1999**, 577. (b) Tsai, M.-H.; Lin, H.-W.; Su, H.-C.; Ke, T.-H.; Wu, C.-c.; Fang, F.-C.; Liao, Y.-L.; Wong, K.-T.; Wu, C.-I. *Adv. Mater.* **2006**, *18*, 1216. (c) Tang, X.; Liu, W.; Wu, J.; Lee, C.-S.; You, J.; Wang, P. *J. Org. Chem.* **2010**, *75*, 7273–7278.

(20) Kato, S.-I.; Noguchi, H.; Kobayashi, A.; Yoshihara, T.; Tobita, S.; Nakamura, Y. *J. Org. Chem.* **2012**, *77*, 9120–9133.

(21) (a) Rao, M. R.; Kumar, K. V. P.; Ravikanth, M. *J. Organomet. Chem.* **2010**, 695, 863–869. (b) Watanabe, M.; Goto, K.; Shibahara, M.; Shinmyozu, T. *J. Org. Chem.* **2010**, *75*, 6104–6114.

(22) Kivala, M.; Boudon, C.; Gisselbrecht, J.-P.; Seiler, P.; Gross, M.; Diederich, F. *Angew. Chem., Int. Ed.* **2007**, *46*, 6357–6360.

(23) (a) Pop, F.; Amacher, A.; Avarvari, N.; Ding, J.; Daku, L. M. L.; Hauser, A.; Koch, M.; Hauser, J.; Liu, S.; Decurtins, S. *Chem.—Eur. J.* **2013**, *19*, 2504–2514. (b) Anant, P.; Lucas, N. T.; Jacob, J. *Org. Lett.* **2008**, *10*, 5533–5536.

(24) Gritzner, G.; Kuta, J. *Pure Appl. Chem.* **1984**, *56*, 461–466.

(25) (a) Frisch, M. J.; Trucks, G. W.; Schlegel, H. B.; Scuseria, G. E.; Robb, M. A.; Cheeseman, J. R.; Scalmani, G.; Barone, V.; Mennucci, B.; Petersson, G. A.; Nakatsuji, H.; Caricato, M.; Li, X.; Hratchian, H. P.; Izmaylov, A. F.; Bloino, J.; Zheng, G.; Sonnenberg, J. L.; Hada, M.; Ehara, M.; Toyota, K.; Fukuda, R.; Hasegawa, J.; Ishida, M.; Nakajima, T.; Honda, Y.; Kitao, O.; Nakai, H.; Vreven, T.; Montgomery, J. A., Jr.; Peralta, J. E.; Ogliaro, F.; Bearpark, M.; Heyd, J. J.; Brothers, E.; Kudin, K. N.; Staroverov, V. N.; Kobayashi, R.; Normand, J.; Raghavachari, K.; Rendell, A.; Burant, J. C.; Iyengar, S. S.; Tomasi, J.; Cossi, M.; Rega, N.; Millam, N. J.; Klene, M.; Knox, J. E.; Cross, J. B.; Bakken, V.; Adamo, C.; Jaramillo, J.; Gomperts, R.; Stratmann, R. E.; Yazyev, O.; Austin, A. J.; Cammi, R.; Pomelli, C.; Ochterski, J. W.; Martin, R. L.; Morokuma, K.; Zakrzewski, V. G.; Voth, G. A.; Salvador, P.; Dannenberg, J. J.; Dapprich, S.; Daniels, A. D.; Farkas, O.; Foresman, J. B.; Ortiz, J. V.; Cioslowski, J.; Fox, D. J. *Gaussian 09*, revision A.02; Gaussian, Inc.: Wallingford, CT, 2009. (b) Lee, C.; Yang, W.; Parr, R. G. *Phys. Rev. B* **1988**, *37*, 785–789. (c) Becke, A. D. *J. Chem. Phys.* **1993**, *98*, 1372–1377.